Journal of Computational Physics 456 (2022) 110954

Contents lists available at ScienceDirect

Journal of Computational Physics

www.elsevier.com/locate/jcp

Improving the accuracy and consistency of the scalar auxiliary variable (SAV) method with relaxation

Maosheng Jiang [a], Zengyan Zhang [b], Jia Zhao [b,*]

[a] School of Mathematics and Statistics, Qingdao University, Qingdao 266071, China
[b] Department of Mathematics & Statistics, Utah State University, Logan, UT, 84322, USA

ARTICLE INFO

Article history:
Received 13 April 2021
Received in revised form 4 December 2021
Accepted 4 January 2022
Available online 13 January 2022

Keywords:
Scalar auxiliary variable (SAV)
Energy stable
Phase field models
Gradient flow system
Relaxation technique

ABSTRACT

The scalar auxiliary variable (SAV) method was introduced by Shen et al. in [36] and has been broadly used to solve thermodynamically consistent PDE problems. By utilizing scalar auxiliary variables, the original PDE problems are reformulated into equivalent PDE problems. The advantages of the SAV approach, such as linearity, unconditionally energy stability, and easy-to-implement, are prevalent. However, there is still an open issue unresolved, i.e., the numerical schemes resulting from the SAV method preserve a "modified" energy law according to the auxiliary variables instead of the original variables. Truncation errors are introduced during numerical calculations so that the numerical solutions of the auxiliary variables are no longer equivalent to their original continuous definitions. In other words, even though the SAV scheme satisfies a modified energy law, it does not necessarily satisfy the energy law of the original PDE models. This paper presents one essential relaxation technique to overcome this issue, which we named the relaxed-SAV (RSAV) method. Our RSAV method penalizes the numerical errors of the auxiliary variables by a relaxation technique. In general, the RSAV method keeps all the advantages of the baseline SAV method and improves its accuracy and consistency noticeably. Several examples have been presented to demonstrate the effectiveness of the RSAV approach.

1. Introduction

Many physical problems, such as interface dynamics [2,24,45], crystallization [12,33], thin films [19,38], polymers [11,18], and liquid crystallization [16,17] could be modeled by gradient flow systems which also agree with the second law of thermodynamics. If the total free energy is known, the gradient flow model could be obtained according to the mobility and the variation of free energy. Because of the nonlinear terms in the governing equation, neither the exact solution nor the numerical solution is easy to obtain. In general, consider the spatial-temporal domain $\Omega_t := \Omega \times (0, T]$. The dissipative dynamics of the state variable ϕ is driven by

$$\partial_t \phi(\mathbf{x}, t) = -\mathcal{G}\frac{\delta \mathcal{E}}{\delta \phi}, \quad (\mathbf{x}, t) \in \Omega_t, \tag{1.1}$$

* Corresponding author.
E-mail address: jia.zhao@usu.edu (J. Zhao).

https://doi.org/10.1016/j.jcp.2022.110954
0021-9991/

where $\mathcal{G}$ is a semi-positive definite operator known as the mobility operator, and $\mathcal{E}$ is a functional of ϕ known as the free energy. The triplet $(\phi, \mathcal{G}, \mathcal{E})$ uniquely defines the dissipative system (gradient flow dynamics). For instance, given $\mathcal{G} = 1$ and $\mathcal{E} = \int_\Omega \frac{\varepsilon^2}{2}|\nabla\phi|^2 + \frac{1}{4}(\phi^2-1)^2 d\mathbf{x}$, with ε as a model parameter, we obtain the following Allen-Cahn equation

$$\partial_t \phi = \varepsilon^2 \Delta\phi - \phi^3 + \phi. \tag{1.2}$$

If we consider $\mathcal{G} = -\Delta$ and $\mathcal{E} = \int_\Omega \frac{\varepsilon^2}{2}|\nabla\phi|^2 + \frac{1}{4}(\phi^2-1)^2 d\mathbf{x}$, we obtain the Cahn-Hilliard equation

$$\partial_t \phi = \Delta(-\varepsilon^2 \Delta\phi + \phi^3 - \phi). \tag{1.3}$$

Given $\mathcal{G} = 1$ and $\mathcal{E} = \int_\Omega D|\nabla\phi|^2 d\mathbf{x}$, we have the heat equation

$$\partial_t \phi = D\Delta\phi, \tag{1.4}$$

where D is the diffusion coefficient.

All these models discussed above have an energy dissipation property. Mainly,

$$\frac{d}{dt}\mathcal{E}(\phi) = -(\frac{\delta\mathcal{E}}{\delta\phi}, \frac{\delta\phi}{\delta t}) = -\Big(\frac{\delta\mathcal{E}}{\delta\phi}, \mathcal{G}\frac{\delta\mathcal{E}}{\delta\phi}\Big) \le 0, \tag{1.5}$$

given the boundary terms are diminished to zero. Here we have used the inner product notation $(f, g) = \int_\Omega fg d\mathbf{x}$, $\forall f, g \in L^2(\Omega)$. Numerical algorithms that solve such models shall also preserve the energy dissipation structure, i.e., follow the thermodynamic physical laws. Numerical schemes that preserve the energy dissipation structure are known as energy stable schemes. And if such structure-preserving doesn't depend on the time step, the numerical schemes are known as unconditionally energy stable.

Many energy stable numerical schemes are proposed to approach the solutions of gradient flow models or dissipative systems. The classical approaches are the fully implicit schemes [15]. Though some of them are unconditionally energy stable, solving such fully implicit schemes is not trivial. Nonlinear problems have to be solved in each time step. However, the existence and uniqueness of the solution usually have strong restrictions on the time step, which prevent those fully implicit numerical schemes from being widely used. One remedy is the convex splitting method [13], which splits the nonlinear terms of free energy into the subtraction of two convex functions. It is easy to check that the convex-splitting schemes are unconditionally energy stable and uniquely solvable. However, the general type of second-order convex splitting schemes is not available. So far, it is only possible to design second-order convex-splitting schemes case-by-case [5,35,38,39]. Meanwhile, there are many other unconditionally energy stable methods, such as stabilization method [33,41], exponential time discretization method [8,29,40]. The stabilization method represents the nonlinear terms explicitly and adds some regularization terms to relax strict constraints for the time step. Similarly, with the convex splitting method, it is usually limited to first-order accuracy. The exponential time discretization (ETD) method shows high-order accuracy by integrating the governing equation over a single time step and uses polynomial interpolations for the nonlinear terms. But the theoretical proofs for energy stability properties of high-order ETD schemes are still missing.

Recently, the numerical method named invariant energy quadratization(IEQ) or energy quadratization(EQ) is proposed [21,22,42–44,46–48]. It is a generalization of the method of Lagrange multipliers or auxiliary variables from [4,23]. The IEQ approach permits us to construct linear, second-order, unconditionally energy stable schemes, and furthermore arbitrarily high-order unconditionally energy stable schemes [20,21]. With many advantages of the IEQ or EQ approach, it usually leads to a coupled system with time-dependent coefficients. As a remedy, the SAV approach [25,30–32,34,36,37] has been proposed by introducing scalar auxiliary variables instead of auxiliary function variables. The SAV method also can be applied to a large class of gradient flow systems, which keeps the advantages of the EQ approach but usually leads to decoupled systems with constant coefficients. These properties make the SAV method easier to implement, so it is highly efficient. Besides, when the researchers applied the SAV approach to many different systems, several modified schemes were developed. Multiple scalar auxiliary variable (MSAV) approach [9] was proposed to solve the phase-field vesicle membrane model where two auxiliary variables were introduced to match two additional penalty terms enforcing the volume and surface area. If using the introduced scalar variable to control both the nonlinear and the explicit linear terms, one highly efficient SAV approach was developed [26], which spent half of the time compared with the original SAV approach while keeping all its other advantages. One stabilized-scalar auxiliary variable (S-SAV) [27] approach was proposed to solve the phase-field surfactant model, which is a decoupled scheme and allowed to be solved step by step. For the phase-field surfactant model, the authors in [50] also presented certain subtle explicit-implicit treatments for stress and convective terms to construct the linear, decoupled, unconditionally energy stable schemes based on the classical SAV approach.

However, there is still a big gap for the IEQ or SAV method, making them not as perfect as expected. Mainly, these two methods preserve a "modified" energy law according to the auxiliary variables instead of the original variables. This inconsistency introduces errors during the computation. In the end, even though the IEQ or SAV schemes preserve the "modified" energy law, they are not necessarily preserving the original energy law, i.e., the energy law for the original PDE models might be violated by the numerical solutions. This is known in the community, but so far, no good remedy is available yet for the SAV schemes, with the IEQ schemes partially addressed in [49]. This motivates our research in this paper. With a novel relaxation step, we effectively penalize the inconsistency between numerical solutions for the auxiliary

variables and their continuous definitions. Thus we name this new approach the relaxed-SAV (RSAV) method. Through the RSAV method, we are able to design novel linear, second-order, unconditionally energy stable schemes, which keep the advantages of the baseline SAV method and preserve the original energy law. It turns out that the relaxation approach effectively improves the accuracy and consistency of the SAV method noticeably.

The rest of this paper is organized as follows. In Section 2, we revisit the baseline SAV method for the general gradient flow system. After that, we propose our remedy: the relaxed SAV method, which we named the RSAV method. The energy stability properties of the RSAV method are proved rigorously in Section 3. Then, we briefly illustrate that the relaxation technique can be easily applied to variations of the SAV method in Section 4. Then in Section 5, several specific examples and numerical tests are provided to verify the accuracy and effectiveness of the proposed relaxed SAV numerical schemes. In the end, we give a brief conclusion.

2. A brief review of the SAV method

Consider the general gradient flow model

$$\frac{\partial \phi}{\partial t} = -\mathcal{G}\frac{\delta \mathcal{E}}{\delta \phi}, \tag{2.1}$$

where ϕ is the state variable, $\mathcal{E}$ is the free energy, and $\mathcal{G}$ is a semi-positive definite operator for dissipative systems (and a skew-symmetric operator for reversible systems or Hamiltonian systems). In the rest of this paper, we consider periodic boundary conditions for simplicity, though all our results can be applied to models with thermodynamically consistent boundary conditions.

For the general gradient flow model (2.1), it has the following energy law

$$\frac{d}{dt}\mathcal{E}(\phi) = (\frac{\delta \mathcal{E}}{\delta \phi}, \frac{\partial \phi}{\partial t}) = -\Big(\frac{\delta \mathcal{E}}{\delta \phi}, \mathcal{G}\frac{\delta \mathcal{E}}{\delta \phi}\Big). \tag{2.2}$$

When $\mathcal{G}$ is semi-positive definite, we have $\frac{d\mathcal{E}}{dt} \le 0$, and when $\mathcal{G}$ is a skew-symmetric operator, we have $\frac{d\mathcal{E}}{dt} = 0$. Here we use the notation, $(f, g) = \int_\Omega fg d\mathbf{x}$, $\forall f, g \in L^2(\Omega)$. The induced norm will be denoted as $\|f\| = \sqrt{(f, f)}$.

Following the notations in [36], we start with a simplified free energy

$$\mathcal{E} = \int_\Omega \Big(\frac{1}{2}\phi \mathcal{L}\phi + F(\phi)\Big) d\mathbf{x}, \tag{2.3}$$

where $\mathcal{L}$ is a linear operator, and F is the bulk free energy density. Also, we denote the identity operator as I that will be used in the rest of this paper. Then the gradient flow model in (2.1) is specified as

$$\partial_t \phi = -\mathcal{G}(\mathcal{L}\phi + F'(\phi)), \tag{2.4}$$

with the following energy law

$$\frac{d\mathcal{E}}{dt} = \int_\Omega \frac{\delta \mathcal{E}}{\delta \phi}\frac{\partial \phi}{\partial t} d\mathbf{x} = -\Big(\mathcal{L}\phi + F'(\phi), \mathcal{G}(\mathcal{L}\phi + F'(\phi))\Big). \tag{2.5}$$

For the SAV method, a scalar auxiliary variable $q(t)$ is introduced as

$$q(t) := Q(\phi) = \sqrt{\int_\Omega (F(\phi) - \frac{1}{2}\gamma_0 \phi^2) d\mathbf{x} + C_0}, \tag{2.6}$$

where $C_0 > 0$ is a constant making sure $Q(\phi)$ is well-defined, i.e., $\int_\Omega (F(\phi) - \frac{1}{2}\gamma_0\phi^2) d\mathbf{x} + C_0 > 0$. Here γ_0 is a regularization parameter that was first introduced in [7]. With the scalar auxiliary variable $q(t)$, the gradient flow model (2.4) is reformulated into an equivalent form

$$\frac{\partial \phi}{\partial t} = -\mathcal{G}\Big(\mathcal{L}\phi + \gamma_0\phi + \frac{q(t)}{Q(\phi)} V(\phi)\Big), \tag{2.7a}$$

$$\frac{dq(t)}{dt} = \frac{1}{2Q(\phi)} \int_\Omega V(\phi)\partial_t \phi d\mathbf{x}, \quad V(\phi) = F'(\phi) - \gamma_0\phi. \tag{2.7b}$$

Denote the modified energy $\hat{E}$ as

$$\hat{E} = \int_\Omega \Big(\frac{1}{2}\phi \mathcal{L}\phi + \frac{1}{2}\gamma_0\phi^2\Big) d\mathbf{x} + q^2 - C_0. \tag{2.8}$$

The reformulated model (2.7) has the following energy law

$$\frac{d\hat{E}}{dt} = \int_{\Omega} \frac{\delta \hat{E}}{\delta \phi}\frac{\partial \phi}{\partial t} d\mathbf{x} + \frac{\delta \hat{E}}{\delta q}\frac{dq}{dt} \tag{2.9a}$$

$$= -\Big(\mathcal{L}\phi + \gamma_0\phi + \frac{q(t)}{Q(\phi)}V(\phi), \mathcal{G}(\mathcal{L}\phi + \gamma_0\phi + \frac{q(t)}{Q(\phi)}V(\phi))\Big). \tag{2.9b}$$

Remark 2.1. With the SAV transformation, numerical algorithms can be introduced to solve the equivalent model in (2.7) that in turn solve the original model in (2.4), since (2.7) and (2.4) are equivalent.

Consider the time domain $[0, T]$, and we discretize it into equally distanced meshes $0 = t_0 < t_1 < \cdots < t_N = T$, with $t_i = i\delta t$ and $\delta t = \frac{T}{N}$. Then we use $(\bullet)^{n+1}$ to represent the numerical approximation of $(\bullet)$ at t_{n+1}. With these notations, we recall the second-order numerical schemes designed for the reformulated model in (2.7). In particular, the following two schemes can be easily obtained.

Scheme 2.1 *(Second-order SAV-BDF2 Scheme).*

$$\frac{3\phi^{n+1} - 4\phi^n + \phi^{n-1}}{2\delta t} = -\mathcal{G}\mu^{n+1}, \tag{2.10a}$$

$$\mu^{n+1} = \mathcal{L}\phi^{n+1} + \gamma_0\phi^{n+1} + \frac{q^{n+1}}{Q(\overline{\phi}^{n+1})}V(\overline{\phi}^{n+1}), \tag{2.10b}$$

$$\frac{3q^{n+1} - 4q^n + q^{n-1}}{2\delta t} = \int_{\Omega} \frac{V(\overline{\phi}^{n+1})}{2Q(\overline{\phi}^{n+1})}\frac{3\phi^{n+1} - 4\phi^n + \phi^{n-1}}{2\delta t} d\mathbf{x}, \tag{2.10c}$$

where $\overline{\phi}^{n+1} = \frac{3}{2}\phi^n - \frac{1}{2}\phi^{n-1}$ and $V(\overline{\phi}^{n+1}) = F'(\overline{\phi}^{n+1}) - \gamma_0\overline{\phi}^{n+1}$.

The SAV-BDF2 Scheme 2.1 has the following discrete energy law.

Theorem 2.1. *The Scheme 2.1 is unconditionally energy stable in the sense that [37]*

$$\begin{aligned}\frac{1}{4}[(\phi^{n+1}, (\mathcal{L} + \gamma_0 I)\phi^{n+1}) + (2\phi^{n+1} - \phi^n, (\mathcal{L} + \gamma_0 I)(2\phi^{n+1} - \phi^n))] + \frac{1}{2}[(q^{n+1})^2 + (2q^{n+1} - q^n)^2] \\ - \frac{1}{4}[(\phi^n, (\mathcal{L} + \gamma_0 I)\phi^n) + (2\phi^n - \phi^{n-1}, (\mathcal{L} + \gamma_0 I)(2\phi^n - \phi^{n-1}))] - \frac{1}{2}[(q^n)^2 + (2q^n - q^{n-1})^2] \\ \leq -\delta t(\mathcal{G}\mu^{n+1}, \mu^{n+1}).\end{aligned}$$

Secondly, if we use the semi-implicit Crank-Nicolson method for the time discretization, we will have the SAV-CN scheme as below.

Scheme 2.2 *(Second-order SAV-CN Scheme).*

$$\frac{\phi^{n+1} - \phi^n}{\delta t} = -\mathcal{G}\mu^{n+\frac{1}{2}}, \tag{2.12a}$$

$$\mu^{n+\frac{1}{2}} = \mathcal{L}\phi^{n+\frac{1}{2}} + \gamma_0\phi^{n+\frac{1}{2}} + \frac{q^{n+\frac{1}{2}}}{Q(\overline{\phi}^{n+\frac{1}{2}})}V(\overline{\phi}^{n+\frac{1}{2}}), \tag{2.12b}$$

$$\frac{q^{n+1} - q^n}{\delta t} = \int_{\Omega} \frac{V(\overline{\phi}^{n+\frac{1}{2}})}{2Q(\overline{\phi}^{n+\frac{1}{2}})}\frac{\phi^{n+1} - \phi^n}{\delta t} d\mathbf{x}, \tag{2.12c}$$

where $\overline{\phi}^{n+\frac{1}{2}} = \frac{3}{2}\phi^n - \frac{1}{2}\phi^{n-1}$ and $V(\overline{\phi}^{n+\frac{1}{2}}) = F'(\overline{\phi}^{n+\frac{1}{2}}) - \gamma_0\overline{\phi}^{n+\frac{1}{2}}$.

The SAV-CN scheme has the following discrete energy law.

Theorem 2.2. *The Scheme 2.2 is unconditionally energy stable in the sense that [37]*

$$\frac{1}{2}(\phi^{n+1}, (\mathcal{L} + \gamma_0 I)\phi^{n+1}) + (q^{n+1})^2 - \frac{1}{2}(\phi^n, (\mathcal{L} + \gamma_0 I)\phi^n) - (q^n)^2 = -\delta t(\mathcal{G}\mu^{n+1}, \mu^{n+1}).$$

3. Our remedy: the relaxed SAV (RSAV) method

Notice the definition in (2.6) tells us $\frac{q(t)}{Q(\phi)} = 1$. Hence, we can observe the two energies (2.3) and (2.8) are equivalent in the PDE level. Meanwhile, the two PDE models (2.4) and (2.7) are equivalent. However, after temporal discretization, the numerical results of $q(t)$ and $Q(\phi)$ are not equal anymore, which means the discrete energies of (2.3) and (2.8) are not necessarily equivalent anymore. The major issue is that q^{n+1} is no longer equal to $Q(\phi^{n+1})$ numerically. Thus, an energy stable scheme that satisfies the modified energy law in (2.8) does not necessarily satisfy the original energy law in (2.3).

To fix the inconsistency issue for q^{n+1} and $Q(\phi^{n+1})$ (that are supposed to be equal as introduced in (2.6)), we propose a relaxation technique to penalize the difference between q^{n+1} and $Q(\phi^{n+1})$. As will be clear in the following sections, the RSAV method introduces negligible extra computational cost, but it inherits all the baseline SAV method's good properties.

If we utilize the semi-implicit BDF2 time marching method, we have the following RSAV-BDF2 scheme.

Scheme 3.1 *(Second-order RSAV-BDF2 Scheme).* We can update ϕ^{n+1} via the following two steps:

- Step 1. Calculate the intermediate solution $(\phi^{n+1}, \tilde{q}^{n+1})$ from the baseline SAV method.

$$\frac{3\phi^{n+1} - 4\phi^n + \phi^{n-1}}{2\delta t} = \mu^{n+1}, \tag{3.1a}$$

$$\mu^{n+1} = -\mathcal{G}\Big(\mathcal{L}\phi^{n+1} + \gamma_0\phi^{n+1} + \frac{\tilde{q}^{n+1}}{Q(\overline{\phi}^{n+1})} V(\overline{\phi}^{n+1})\Big), \tag{3.1b}$$

$$\frac{3\tilde{q}^{n+1} - 4q^n + q^{n-1}}{2\delta t} = \int_\Omega \frac{V(\overline{\phi}^{n+1})}{2Q(\overline{\phi}^{n+1})} \frac{3\phi^{n+1} - 4\phi^n + \phi^{n-1}}{2\delta t} d\mathbf{x}, \tag{3.1c}$$

  Where $\overline{\phi}^{n+1} = \frac{3}{2}\phi^n - \frac{1}{2}\phi^{n-1}$ and $V(\overline{\phi}^{n+1}) = F'(\overline{\phi}^{n+1}) - \gamma_0\overline{\phi}^{n+1}$.
- Step 2. Update the scalar auxiliary variable q^{n+1} via a relaxation step as

$$q^{n+1} = \xi_0\tilde{q}^{n+1} + (1-\xi_0)Q(\phi^{n+1}), \quad \xi_0 \in \mathcal{V}. \tag{3.2}$$

  Here, $\mathcal{V}$ is a set defined by $\mathcal{V} = \mathcal{V}_1 \cap \mathcal{V}_2$, where

$$\mathcal{V}_1 = \{\xi | \xi \in [0,1]\}, \tag{3.3a}$$

$$\mathcal{V}_2 = \Big\{\xi | \frac{1}{2}[(q^{n+1})^2 + (2q^{n+1} - q^n)^2] - \frac{1}{2}[(\tilde{q}^{n+1})^2 + (2\tilde{q}^{n+1} - q^n)^2] \le \delta t\eta(\mathcal{G}\mu^{n+1}, \mu^{n+1}), \quad q^{n+1} = \xi\tilde{q}^{n+1} + (1-\xi)Q(\phi^{n+1})\Big\}. \tag{3.3b}$$

  Here, $\eta \in [0,1]$ is an artificial parameter that can be manually assigned.

Several vital observations for Scheme 3.1 are given as follows.

Remark 3.1. We emphasis that the set $\mathcal{V}$ in (3.2) is non-empty by noticing $1 \in \mathcal{V}$.

Remark 3.2. Scheme 3.1 is second-order accurate in time. In particular, the relaxation step in (3.2) does not affect the order of accuracy in time. Notice $\tilde{q}^{n+1} = Q(\phi(\mathbf{x}, t_{n+1})) + O(\delta t^2)$ and $Q(\phi^{n+1}) = Q(\phi(\mathbf{x}, t_{n+1})) + O(\delta t^2)$. Hence

$$q^{n+1} = \xi_0\tilde{q}^{n+1} + (1-\xi_0)Q(\phi^{n+1}) = Q(\phi(\mathbf{x}, t_{n+1})) + O(\delta t^2).$$

Remark 3.3 *(Optimal choice for ξ_0).* Here we explain the optimal choice for the relaxation parameter ξ_0 in (3.2). ξ_0 can be chosen as a solution of the following optimization problem,

$$\xi_0 = \min_{\xi\in[0,1]} \xi, \quad \text{s.t. } \frac{1}{2}[(q^{n+1})^2 + (2q^{n+1} - q^n)^2] - \frac{1}{2}[(\tilde{q}^{n+1})^2 + (2\tilde{q}^{n+1} - q^n)^2] \le \delta t\eta(\mathcal{G}\mu^{n+1}, \mu^{n+1}), \tag{3.4}$$

with $q^{n+1} = \xi\tilde{q}^{n+1} + (1-\xi)Q(\phi^{n+1})$. This can be simplified as

$$\xi_0 = \min_{\xi\in[0,1]} \xi, \quad \text{s.t. } a\xi^2 + b\xi + c \le 0, \tag{3.5}$$

where the coefficients are

$$a = \frac{5}{2}(\tilde{q}^{n+1} - Q(\phi^{n+1}))^2,$$
$$b = (\tilde{q}^{n+1} - Q(\phi^{n+1}))(5Q(\phi^{n+1}) - 2q^n),$$
$$c = \frac{1}{2}[(Q(\phi^{n+1}))^2 + (2Q(\phi^{n+1}) - q^n)^2 - (\tilde{q}^{n+1})^2 - (2\tilde{q}^{n+1} - q^n)^2] - \delta t\eta(\mathcal{G}\mu^{n+1}, \mu^{n+1}).$$

Notice the fact $\delta t\eta(\mathcal{G}\mu^{n+1}, \mu^{n+1}) \geq 0$, and $a + b + c \leq 0$. Given $a \neq 0$, the optimization problem in (3.5) can be solved as

$$\xi_0 = \max\{0, \frac{-b - \sqrt{b^2 - 4ac}}{2a}\}.$$

Remark 3.4. The RSAV method could refrain the SAV from constantly deviating from the original definition. As presented in Step 2, we could see that $\xi_0 \in [0,1]$, when ξ_0 =1, i.e., $q^{n+1} = \tilde{q}^{n+1}$, this is the original SAV method; when ξ_0 =0, $q^{n+1} = Q(\phi^{n+1})$ and the discrete energies of (2.3) and (2.8) are equivalent, and when $\xi_0 \in (0,1)$, then q^{n+1} is a linear combination of $\tilde{q}^{n+1}$ and $Q(\phi^{n+1})$. This will bring the discrete energy of (2.8) closer to the discrete energy of (2.3) by penalizing the difference between the numerical approximation of the scalar auxiliary variable, $\tilde{q}^{n+1}$ and its original definition, $Q(\phi^{n+1})$.

Theorem 3.1. *The Scheme 3.1 is unconditionally energy stable.*

Proof. According to the Theorem 2.1, we could get

$$\frac{1}{4}[(\phi^{n+1}, (\mathcal{L} + \gamma_0 I)\phi^{n+1}) + (2\phi^{n+1} - \phi^n, (\mathcal{L} + \gamma_0 I)(2\phi^{n+1} - \phi^n))] + \frac{1}{2}[(\tilde{q}^{n+1})^2 + (2\tilde{q}^{n+1} - q^n)^2]$$
$$- \frac{1}{4}[(\phi^n, (\mathcal{L} + \gamma_0 I)\phi^n) + (2\phi^n - \phi^{n-1}, (\mathcal{L} + \gamma_0 I)(2\phi^n - \phi^{n-1}))] - \frac{1}{2}[(q^n)^2 + (2q^n - q^{n-1})^2]$$
$$\leq -\delta t(\mathcal{G}\mu^{n+1}, \mu^{n+1}),$$

for the first step of the Scheme 3.1. At the same time, we could get

$$\frac{1}{2}[(q^{n+1})^2 + (2q^{n+1} - q^n)^2] - \frac{1}{2}[(\tilde{q}^{n+1})^2 + (2\tilde{q}^{n+1} - q^n)^2] \leq \delta t\eta(\mathcal{G}\mu^{n+1}, \mu^{n+1}), \tag{3.8}$$

from (3.2). Adding the above two equations together, we could have

$$\frac{1}{4}[(\phi^{n+1}, (\mathcal{L} + \gamma_0 I)\phi^{n+1}) + (2\phi^{n+1} - \phi^n, (\mathcal{L} + \gamma_0 I)(2\phi^{n+1} - \phi^n))] + \frac{1}{2}[(q^{n+1})^2 + (2q^{n+1} - q^n)^2]$$
$$- \frac{1}{4}[(\phi^n, (\mathcal{L} + \gamma_0 I)\phi^n) + (2\phi^n - \phi^{n-1}, (\mathcal{L} + \gamma_0 I)(2\phi^n - \phi^{n-1}))] - \frac{1}{2}[(q^n)^2 + (2q^n - q^{n-1})^2]$$
$$\leq -\delta t(1 - \eta)(\mathcal{G}\mu^{n+1}, \mu^{n+1}) \leq 0,$$

since $1 - \eta \geq 0$. This completes the proof. □

Scheme 3.2 *(Second-order RSAV-CN Scheme).* We update ϕ^{n+1} via the following two steps:

- Step 1. Calculate the intermediate solution $(\phi^{n+1}, \tilde{q}^{n+1})$ using the baseline SAV-CN method as below.

$$\frac{\phi^{n+1} - \phi^n}{\delta t} = -\mathcal{G}\mu^{n+\frac{1}{2}}, \tag{3.10a}$$
$$\mu^{n+\frac{1}{2}} = \mathcal{L}\phi^{n+\frac{1}{2}} + \gamma_0\phi^{n+\frac{1}{2}} + \frac{\tilde{q}^{n+\frac{1}{2}}}{Q(\overline{\phi}^{n+\frac{1}{2}})}V(\overline{\phi}^{n+\frac{1}{2}}), \tag{3.10b}$$
$$\frac{\tilde{q}^{n+1} - q^n}{\delta t} = \int_\Omega \frac{V(\overline{\phi}^{n+\frac{1}{2}})}{2Q(\overline{\phi}^{n+\frac{1}{2}})}\frac{\phi^{n+1} - \phi^n}{\delta t}d\mathbf{x}. \tag{3.10c}$$

- Step 2. Update the scalar auxiliary variable q^{n+1} as

$$q^{n+1} = \xi_0\tilde{q}^{n+1} + (1 - \xi_0)Q(\phi^{n+1}), \quad \xi_0 \in \mathcal{V}, \tag{3.11}$$

with the feasible set $\mathcal{V}$ defined as $\mathcal{V} = \mathcal{V}_1 \cap \mathcal{V}_2$, where

$$\mathcal{V}_1 = \{\xi | \xi \in [0, 1]\}, \tag{3.12a}$$
$$\mathcal{V}_2 = \left\{\xi | (q^{n+1})^2 - (\tilde{q}^{n+1})^2 \leq \delta t\eta(\mathcal{G}\mu^{n+\frac{1}{2}}, \mu^{n+\frac{1}{2}}), \quad q^{n+1} = \xi\tilde{q}^{n+1} + (1 - \xi)Q(\phi^{n+1})\right\}. \tag{3.12b}$$

Similarly, we have the following critical observations for Scheme 3.2.

Remark 3.5. The set $\mathcal{V}$ in (3.11) is non-empty, given that $1 \in \mathcal{V}$.

Remark 3.6. The Scheme 3.2 is second-order accurate in time. Because the relaxation step in (3.11) doesn't not affect the order of accuracy. Notice $\tilde{q}^{n+1} = Q(\phi(\mathbf{x}, t_{n+1})) + O(\delta t^2)$ and $Q(\Phi^{n+1}) = Q(\phi(\mathbf{x}, t_{n+1})) + O(\delta t^2)$. Hence

$$q^{n+1} = \xi_0 \tilde{q}^{n+1} + (1-\xi_0) Q(\phi^{n+1}) = Q(\phi(\mathbf{x}, t_{n+1})) + O(\delta t^2).$$

Remark 3.7 *(Optimal choice for ξ_0).* Here we elaborate the optimal choice for the relaxation parameter ξ_0. We can choose ξ_0 as the solution of the following optimization problem

$$\xi_0 = \min_{\xi \in [0,1]} \xi, \quad \text{s.t. } (q^{n+1})^2 - (\tilde{q}^{n+1})^2 \le \delta t \eta(\mu^{n+\frac{1}{2}}, \mathcal{G}\mu^{n+\frac{1}{2}}). \tag{3.13}$$

This can be simplified as

$$\xi_0 = \min_{\xi \in [0,1]} \xi, \quad \text{s.t. } a\xi^2 + b\xi + c \le 0, \tag{3.14}$$

where the coefficients are

$$a = (\tilde{q}^{n+1} - Q(\phi^{n+1}))^2, \quad b = 2\big(\tilde{q}^{n+1} - Q(\phi^{n+1})\big) Q(\phi^{n+1}), \tag{3.15a}$$

$$c = [Q(\phi^{n+1})]^2 - (\tilde{q}^{n+1})^2 - \delta t \eta(\mu^{n+\frac{1}{2}}, \mathcal{G}\mu^{n+\frac{1}{2}}). \tag{3.15b}$$

Notice $a + b + c < 0$. Given $a \neq 0$, the solution to (3.13) is given as

$$\xi_0 = \max\{0, \frac{-b - \sqrt{b^2 - 4ac}}{2a}\}.$$

Theorem 3.2. *The Scheme 3.2 is unconditionally energy stable.*

Proof. For the step in 3.10, thanks to the Theorem 2.2, we could get

$$\frac{1}{2}(\phi^{n+1}, (\mathcal{L} + \gamma_0 I)\phi^{n+1}) + (\tilde{q}^{n+1})^2 - \frac{1}{2}(\phi^n, (\mathcal{L} + \gamma_0 I)\phi^n) - (q^n)^2 = -\delta t(\mathcal{G}\mu^{n+\frac{1}{2}}, \mu^{n+\frac{1}{2}}). \tag{3.16}$$

From (3.11), we know

$$(q^{n+1})^2 - (\tilde{q}^{n+1})^2 \le \delta t \eta(\mathcal{G}\mu^{n+\frac{1}{2}}, \mu^{n+\frac{1}{2}}). \tag{3.17}$$

Adding two equations (3.16) and (3.17), and acknowledging the inequality $1 - \eta \ge 0$, we could arrive at

$$\begin{aligned}\frac{1}{2}(\phi^{n+1}, (\mathcal{L} + \gamma_0 I)\phi^{n+1}) + (q^{n+1})^2 - \frac{1}{2}(\phi^n, (\mathcal{L} + \gamma_0 I)\phi^n) - (q^n)^2 \\ \le -\delta t(1-\eta)(\mathcal{G}\mu^{n+\frac{1}{2}}, \mu^{n+\frac{1}{2}}) \le 0.\end{aligned}$$

This completes the proof. □

4. Relaxation techniques for the variations of the SAV method

Given the popularity of the SAV method, several variations are proposed to apply in different situations [3,9,10,14,20,28]. Since our proposed relaxation technique doesn't restrict the specific form of the scalar auxiliary variables, our RSAV method can be easily extended to some SAV variations.

As one example, we explain the idea based on the multiple scalar auxiliary variable (MSAV) method [9]. To present the MSAV method [9], we consider a more general form of the free energy

$$\mathcal{E} = \int_\Omega \Big(\frac{1}{2}\phi\mathcal{L}\phi + \sum_{i=1}^{k} F_i(\phi)\Big) d\mathbf{x}, \tag{4.1}$$

where $\mathcal{L}$ is a linear operator, and $F_i(\phi)$, $i = 1, 2, \cdots, k$ are the bulk potentials. Then the general gradient flow model is given as

$$\frac{\partial \phi}{\partial t} = -\mathcal{G}\Big[\mathcal{L}\phi + \sum_{i=1}^{k} F_i'(\phi)\Big], \tag{4.2}$$

which has the following energy law

$$\frac{d}{dt}\mathcal{E}(\phi) = (\frac{\delta \mathcal{E}}{\delta \phi}, \frac{\partial \phi}{\partial t}) = -\Big(\Big[\mathcal{L}\phi + \sum_{i=1}^{k} F_i'(\phi)\Big], \mathcal{G}\Big[\mathcal{L}\phi + \sum_{i=1}^{k} F_i'(\phi)\Big]\Big). \tag{4.3}$$

When $\mathcal{G}$ is semi-positive definite, we have $\frac{d\mathcal{E}}{dt} \le 0$, and when $\mathcal{G}$ is a skew-symmetric operator, we have $\frac{d\mathcal{E}}{dt} = 0$. For the problem in (4.2), multiple scalar auxiliary variables are introduced as

$$q_i(t) := Q_i(\phi) = \sqrt{\int_\Omega (F_i(\phi) - \frac{1}{2}\gamma_i \phi^2) d\mathbf{x} + C_i}, \quad i = 1, 2, \cdots, k. \tag{4.4}$$

Here C_i are positive constants that make sure $q_i(t)$ are well defined. And γ_i are the regularization constants [7]. With the scalar auxiliary variables $q_i(t)$, the gradient flow model (4.2) can be reformulated into an equivalent form

$$\frac{\partial \phi}{\partial t} = -\mathcal{G}\Big(\mathcal{L}\phi + \sum_{i=1}^{k} \gamma_i \phi + \sum_{i=1}^{k} \frac{q_i(t)}{Q_i(\phi)} V_i(\phi)\Big), \tag{4.5a}$$

$$\frac{dq_j(t)}{dt} = \frac{1}{2Q_j(\phi)} \int_\Omega V_j(\phi)\partial_t \phi d\mathbf{x}, \quad j = 1, 2, \cdots, k, \tag{4.5b}$$

where $V_i(\phi) = F_i'(\phi) - \gamma_i \phi$, $i = 1, ..., k$.

With the introduction of the multiple scalar auxiliary variables in (4.4), we can get the modified free energy as:

$$\hat{E} = \int_\Omega \Big(\frac{1}{2}\phi \mathcal{L}\phi + \sum_{i=1}^{k} \frac{\gamma_i}{2}\phi^2\Big) d\mathbf{x} + \sum_{i=1}^{k} (q_i^2 - C_i). \tag{4.6}$$

For the reformulated model (4.5), it has the following energy law

$$\begin{aligned} \frac{d\hat{E}}{dt} &= \int_\Omega \frac{\delta \hat{E}}{\delta \phi}\frac{\partial \phi}{\partial t} d\mathbf{x} + \sum_{i=1}^{k} \frac{\delta \hat{E}}{\delta q_i}\frac{dq_i}{dt} \\ &= -\Big(\Big[\mathcal{L}\phi + \sum_{i=1}^{k}\gamma_i\phi + \sum_{i=1}^{k}\frac{q_i(t)}{Q_i(\phi)}V_i(\phi)\Big], \mathcal{G}\Big[\mathcal{L}\phi + \sum_{i=1}^{k}\gamma_i\phi + \sum_{i=1}^{k}\frac{q_i(t)}{Q_i(\phi)}V_i(\phi)\Big]\Big). \end{aligned}$$

In a similar manner, we introduce the relaxation technique to the MASV method to fix the inconsistency issues between $q_i(t)$ and $Q_i(\phi)$ after discretization. The two second-order MSAV schemes could be improved as follows.

Scheme 4.1 *(Second-order RMSAV-BDF2 Scheme).* We update ϕ^{n+1} via the following two steps:

- Step 1, Calculate the intermediate solution $(\phi^{n+1}, \tilde{q}^{n+1})$ using the MSAV-BDF2 method as below.

$$\frac{3\phi^{n+1} - 4\phi^n + \phi^{n-1}}{2\delta t} = -\mathcal{G}\mu^{n+1}, \tag{4.8a}$$

$$\mu^{n+1} = \mathcal{L}\phi^{n+1} + \sum_{i=1}^{k}\gamma_i\phi^{n+1} + \sum_{i}^{k}\frac{\tilde{q}_i^{n+1}}{Q_i(\overline{\phi}^{n+1})}V_i(\overline{\phi}^{n+1}), \tag{4.8b}$$

$$\frac{3\tilde{q}_j^{n+1} - 4q_j^n + q_j^{n-1}}{2\delta t} = \int_\Omega \frac{V_j(\overline{\phi}^{n+1})}{2Q_j(\overline{\phi}^{n+1})}\frac{3\phi^{n+1} - 4\phi^n + \phi^{n-1}}{2\delta t} d\mathbf{x}, \quad j = 1, 2, \cdots, k, \tag{4.8c}$$

  where $\overline{\phi}^{n+1} = \frac{3}{2}\phi^n - \frac{1}{2}\phi^{n-1}$ and $V_i(\overline{\phi}^{n+1}) = F_i'(\overline{\phi}^{n+1}) - \gamma_i\overline{\phi}^{n+1}$, $i = 1, 2, \cdots, k$.
- Step 2, update the k scalar auxiliary variables as

$$q_i^{n+1} = \xi_0 \tilde{q}_i^{n+1} + (1 - \xi_0) Q_i(\phi^{n+1}), \quad i = 1, 2, \cdots, k, \quad \xi_0 \in \mathcal{V}, \tag{4.9}$$

where the feasible set $\mathcal{V}$ is defined as $\mathcal{V} = \mathcal{V}_1 \cap \mathcal{V}_2$ with

$$\mathcal{V}_1 = \{\xi | \xi \in [0,1]\}, \tag{4.10a}$$

$$\mathcal{V}_2 = \Big\{\xi | \frac{1}{2}\sum_{i=1}^{k}\Big[(q_i^{n+1})^2 + (2q_i^{n+1} - q_i^n)^2 - ((\tilde{q}_i^{n+1})^2 + (2\tilde{q}_i^{n+1} - q_i^n)^2)\Big] \leq \delta t \eta(\mathcal{G}\mu^{n+1}, \mu^{n+1}), \quad q_i^{n+1} = \xi\tilde{q}_i^{n+1} + (1-\xi)Q(\phi^{n+1}), i = 1, 2, \cdots, k\Big\}, \quad \eta \in [0,1]. \tag{4.10b}$$

Remark 4.1 *(Optimal choice for ξ_0).* Similarly, we can propose an optimal choice for the relaxation parameter ξ_0 as the solution to an optimization problem. And in the end,

$$\xi_0 = \max\{0, \frac{-b - \sqrt{b^2 - 4ac}}{2a}\},$$

with the coefficients given by

$$a = \frac{5}{2}\sum_{i=1}^{k}(\tilde{q}_i^{n+1} - Q_i(\phi^{n+1}))^2,$$

$$b = \sum_{i=1}^{k}(\tilde{q}_i^{n+1} - Q_i(\phi^{n+1}))(5Q_i(\phi^{n+1}) - 2q_i^n),$$

$$c = \frac{1}{2}\sum_{i=1}^{k}[(Q_i(\phi^{n+1}))^2 + (2Q_i(\phi^{n+1}) - q_i^n)^2 - (\tilde{q}_i^{n+1})^2 - (2\tilde{q}_i^{n+1} - q_i^n)^2] - \delta t\eta(\mathcal{G}\mu^{n+1}, \mu^{n+1}).$$

Theorem 4.1. *The Scheme 4.1 is unconditionally energy stable.*

Proof. For the first step of the Scheme 4.1, we could get

$$\begin{aligned}
&\frac{1}{4}[(\phi^{n+1}, (\mathcal{L} + \sum_{i=1}^{k}\gamma_i I)\phi^{n+1}) + (2\phi^{n+1} - \phi^n, (\mathcal{L} + \sum_{i=1}^{k}\gamma_i I)(2\phi^{n+1} - \phi^n))] \\
&- \frac{1}{4}[(\phi^n, (\mathcal{L} + \sum_{i=1}^{k}\gamma_i I)\phi^n) + (2\phi^n - \phi^{n-1}, (\mathcal{L} + \sum_{i=1}^{k}\gamma_i I)(2\phi^n - \phi^{n-1}))] \\
&+ \frac{1}{2}\sum_{i=1}^{k}[(\tilde{q}_i^{n+1})^2 + (2\tilde{q}_i^{n+1} - q_i{}^n)^2] - \frac{1}{2}\sum_{i=1}^{k}[(q_i{}^n)^2 + (2q_i{}^n - q_i{}^{n-1})^2] \\
&\leq -\delta t(\mathcal{G}\mu^{n+1}, \mu^{n+1}).
\end{aligned}$$

At the same time, we know from (4.9), we could know

$$\frac{1}{2}\sum_{i=1}^{k}[(q_i{}^{n+1})^2 + (2q_i{}^{n+1} - q^n)^2] - \frac{1}{2}\sum_{i=1}^{k}[(\tilde{q}_i^{n+1})^2 + (2\tilde{q}_i^{n+1} - q_i{}^n)^2] \leq \delta t\eta(\mathcal{G}\mu^{n+1}, \mu^{n+1}). \tag{4.13}$$

Adding the above two equations together, we could have

$$\begin{aligned}
&\frac{1}{4}[(\phi^{n+1}, (\mathcal{L} + \sum_{i=1}^{k}\gamma_i I)\phi^{n+1}) + (2\phi^{n+1} - \phi^n, (\mathcal{L} + \sum_{i=1}^{k}\gamma_i I)(2\phi^{n+1} - \phi^n))] \\
&- \frac{1}{4}[(\phi^n, (\mathcal{L} + \sum_{i=1}^{k}\gamma_i I)\phi^n) + (2\phi^n - \phi^{n-1}, (\mathcal{L} + \sum_{i=1}^{k}\gamma_i I)(2\phi^n - \phi^{n-1}))] \\
&+ \frac{1}{2}\sum_{i=1}^{k}[(q_i{}^{n+1})^2 + (2q_i{}^{n+1} - q_i{}^n)^2] - \frac{1}{2}\sum_{i=1}^{k}[(q_i{}^n)^2 + (2q_i{}^n - q_i{}^{n-1})^2] \\
&\leq -\delta t(1-\eta)(\mathcal{G}\mu^{n+1}, \mu^{n+1}) \leq 0,
\end{aligned}$$

by using the fact $1 - \eta \geq 0$. This completes the proof. □

Then, if we use the semi-implicit CN time discretization, we can obtain the following second-order scheme.

Scheme 4.2 *(Second-order RMSAV-CN Scheme).* We update ϕ^{n+1} via the following two steps:

- Step 1. Calculate the intermediate solution

$$\frac{\phi^{n+1}-\phi^n}{\delta t} = -\mathcal{G}\mu^{n+\frac{1}{2}}, \tag{4.15a}$$

$$\mu^{n+\frac{1}{2}} = \mathcal{L}\phi^{n+\frac{1}{2}} + \sum_{i=1}^{k}\gamma_i\phi^{n+\frac{1}{2}} + \sum_{i=1}^{k}\frac{\tilde{q}_i^{n+\frac{1}{2}}}{Q_i(\overline{\phi}^{n+\frac{1}{2}})}V_i(\overline{\phi}^{n+\frac{1}{2}}), \tag{4.15b}$$

$$\frac{\tilde{q}_j^{n+1}-q_j^n}{\delta t} = \int_\Omega \frac{V_j(\overline{\phi}^{n+\frac{1}{2}})}{2Q_j(\overline{\phi}^{n+\frac{1}{2}})}\frac{\phi^{n+1}-\phi^n}{\delta t}d\mathbf{x}, \quad j=1,2,\cdots,k. \tag{4.15c}$$

- Step 2. Update the scalar auxiliary variable as

$$q_i{}^{n+1} = \xi_0\tilde{q}_i^{n+1} + (1-\xi_0)Q_i(\phi^{n+1}), \quad i=1,2,\cdots,k, \quad \xi_0\in\mathcal{V}, \tag{4.16}$$

with the feasible set V defined as $\mathcal{V}=\mathcal{V}_1\cap\mathcal{V}_2$, where

$$\mathcal{V}_1 = \{\xi|\xi\in[0,1]\}, \tag{4.17a}$$

$$\mathcal{V}_2 = \Big\{\xi|\sum_{i=1}^{k}\Big[(q_i^{n+1})^2-(\tilde{q}_i^{n+1})^2\Big]\le\delta t\eta(\mathcal{G}\mu^{n+\frac{1}{2}},\mu^{n+\frac{1}{2}}), \quad q_i^{n+1}=\xi\tilde{q}_i^{n+1}+(1-\xi)Q(\phi^{n+1}), \quad i=1,2,\cdots,k\Big\}, \quad \eta\in[0,1]. \tag{4.17b}$$

Remark 4.2. Similarly, the optimal choice for the relaxation parameter can be calculated as $\xi_0=\max\{0,\frac{-b-\sqrt{b^2-4ac}}{2a}\}$ with the coefficients given by

$$a=\sum_{i=1}^{k}(\tilde{q}_i^{n+1}-Q_i(\phi^{n+1}))^2, \quad b=\sum_{i=1}^{k}2\big(\tilde{q}_i^{n+1}-Q_i(\phi^{n+1})\big)Q_i(\phi^{n+1}), \tag{4.18a}$$

$$c=\sum_{i=1}^{k}[Q_i(\phi^{n+1})]^2-\sum_{i=1}^{k}(\tilde{q}_i^{n+1})^2-\delta t\eta(\mu^{n+\frac{1}{2}},\mathcal{G}\mu^{n+\frac{1}{2}}). \tag{4.18b}$$

Theorem 4.2. *The Scheme 4.2 is unconditionally energy stable.*

Proof. For the first step of (4.15), we could get

$$(\phi^{n+1},(\mathcal{L}+\sum_{i=1}^{k}\gamma_i I)\phi^{n+1})+\sum_{i=1}^{k}(\tilde{q}_i^{n+1})^2-(\phi^n,(\mathcal{L}+\sum_{i=1}^{k}\gamma_i I)\phi^n)-\sum_{i=1}^{k}(q_i{}^n)^2=-\delta t(\mathcal{G}\mu^{n+\frac{1}{2}},\mu^{n+\frac{1}{2}}).$$

From (4.16), we know

$$\sum_{i=1}^{k}(q_i{}^{n+1})^2-\sum_{i=1}^{k}(\tilde{q}_i^{n+1})^2\le\delta t\eta(\mathcal{G}\mu^{n+\frac{1}{2}},\mu^{n+\frac{1}{2}}). \tag{4.19}$$

Adding above two equations, and using $1-\eta\ge 0$, we could arrive at

$$(\phi^{n+1},(\mathcal{L}+\sum_{i=1}^{k}\gamma_i I)\phi^{n+1})+\sum_{i=1}^{k}(\tilde{q}_i^{n+1})^2-(\phi^n,(\mathcal{L}+\sum_{i=1}^{k}\gamma_i I)\phi^n)-\sum_{i=1}^{k}(q_i{}^n)^2\le-\delta t(1-\eta)(\mathcal{G}\mu^{n+\frac{1}{2}},\mu^{n+\frac{1}{2}})\le 0.$$

This completes the proof. □

As another example, the relaxation technique can be easily applied to the Runge-Kutta SAV methods [1,20]. The details are omitted for brevity. Interested readers are encouraged to explore the schemes.

Meanwhile, there are still some open problems to be addressed. The SAV method has also been extended for solving the dispersive equations like the Schrödinger/Gross-Pitaevskii equation [3,14]. Applying this relaxation technique to such problems doesn't seem straightforward since the dispersive equations require the preservation of the invariants. How to refrain the difference between the scalar auxiliary variable and its original definition numerically for the dispersive equations is still an open problem. Besides, the SAV method has also been extended to study the time and space fractional PDEs [10,28]. How to resolve the inconsistency issues of the SAV method for these fractional problems also brings huge challenges and opportunities. We plan to address these issues in our future research.

5. Numerical results

In this section, we implement the proposed numerical algorithms and apply them to several classical phase-field models that include the Allen-Cahn (AC) equation, the Cahn-Hilliard (CH) equation, the Molecular Beam Epitaxy (MBE) model, the phase-field crystal (PFC) model and the diblock copolymer model.

For simplicity, we only consider the phase-field models with periodic boundary conditions. However, we emphasize that our proposed algorithms apply to other thermodynamically consistent boundary conditions that satisfy the energy dissipation laws. Given the periodic boundary conditions, we use the Fourier pseudo-spectral method for spatial discretization. Let N_x, N_y be two positive even integers. The spatial domain $\Omega = [0, L_x] \times [0, L_y]$ is uniformly partitioned with mesh size $h_x = L_x/N_x, h_y = L_y/N_y$ and

$$\Omega_h = \left\{(x_j, y_k) | x_j = jh_x,\ y_k = kh_y,\ 0 \le j \le N_x - 1, 0 \le k \le N_y - 1\right\}.$$

The details for spatial discretization are omitted. Interested readers can refer to our previous work [6]. Also, given the BDF2 and CN schemes are both second-order accurate, we only compare the baseline SAV-CN scheme and the RSAV-CN scheme in this paper.

5.1. Allen-Cahn equation

In the first example, we consider the Allen-Cahn equation. Consider the free energy $\mathcal{E} = \int_\Omega \frac{\varepsilon^2}{2}|\nabla\phi|^2 + \frac{1}{4}(\phi^2 - 1)^2 d\mathbf{x}$, with mobility operator $\mathcal{G} = 1$, the general gradient flow model in (2.1) reduces to the corresponding Allen-Cahn equation

$$\partial_t \phi = -\lambda(-\varepsilon^2 \Delta\phi + \phi^3 - \phi). \tag{5.1}$$

In the SAV formulation, we introduce the scalar auxiliary variable

$$q(t) := Q(\phi(\mathbf{x}, t)) = \sqrt{\int_\Omega \frac{1}{4}(\phi^2 - 1 - \gamma_0)^2 d\mathbf{x} + C}.$$

Then the SAV reformulated equations read as

$$\partial_t \phi = -\lambda\Big[-\varepsilon^2 \Delta\phi + \gamma_0\phi + \frac{q(t)}{Q(\phi)} V(\phi)\Big], \quad V(\phi) = \phi(\phi^2 - 1 - \gamma_0), \tag{5.2a}$$

$$\frac{d}{dt} q(t) = \int_\Omega \frac{V(\phi)}{2Q(\phi)} \partial_t \phi d\mathbf{x}. \tag{5.2b}$$

We verify that the relaxed SAV-CN scheme is second-order accurate in time. Consider the domain $\Omega = [0, 1]^2$, and we pick the smooth initial condition

$$\phi(x, y, t = 0) = 0.01 \cos(2\pi x) \cos(2\pi y), \tag{5.3}$$

and set the model parameters: $\varepsilon = 0.01$ and $\lambda = 1$. To solve the AC equation in (5.2), we use uniform meshes $N_x = N_y = 128$, and numerical parameters $C_0 = 1$, $\eta = 0.95$, and $\gamma_0 = 1$.

Given the analytical solutions are unknown, we calculate the error as the difference between the numerical solutions using the current time step and the numerical solutions using the adjacent finer time step. The numerical errors in L^2 norm with various time steps are summarized in Fig. 5.1. A second-order convergence for the numerical solutions of ϕ and q are both observed.

Next, we conduct a detailed comparison between the baseline SAV-CN scheme and the RSAV-CN scheme. We use the same parameters as in the example above. Consider the domain $\Omega = [0, L_x] \times [0, L_y]$, and choose the initial condition as

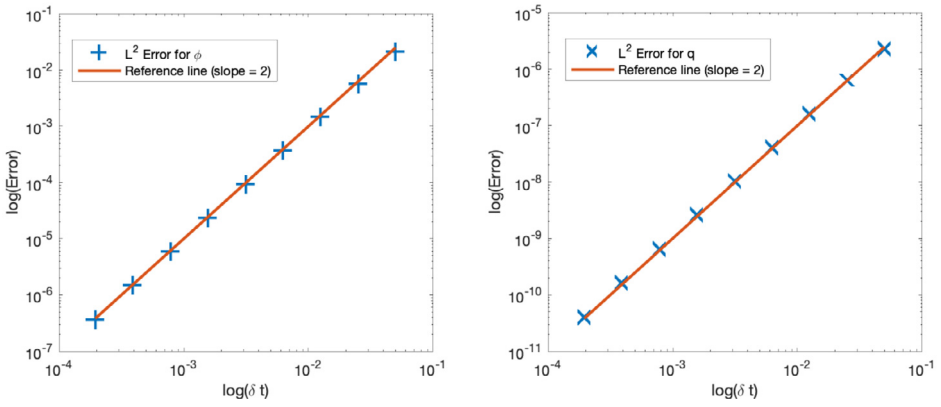

(a) Time step refinement test for ϕ (b) Time step refinement test for q

Fig. 5.1. Time step mesh refinement tests of RSAV-CN scheme for solving the Allen-Cahn equation. This figure indicates that the proposed RSAV-CN algorithm is second-order accuracy in time when solving the Allen-Cahn equation.

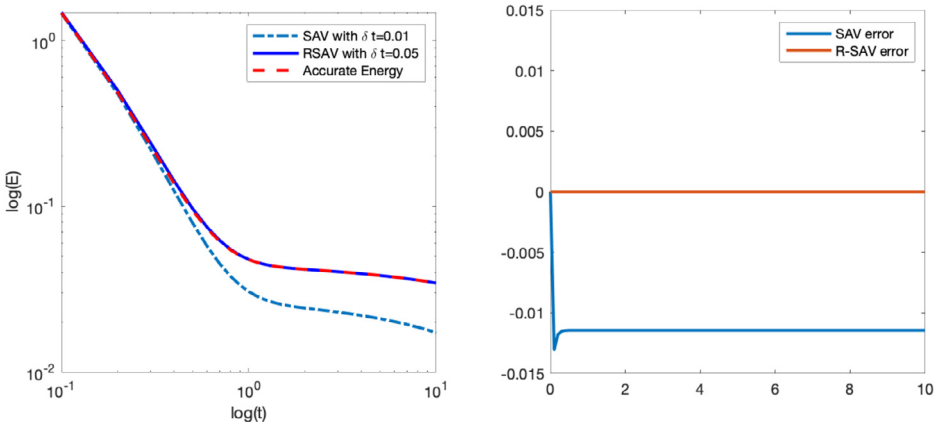

(a) Log-log plot for the energy evolution (b) Numerical results of $q(t)-Q(\phi(\mathbf{x},t))$

Fig. 5.2. A comparison between the baseline SAV method and the relaxed SAV method in solving the Allen-Cahn equation. In (a) the numerical energies using the baseline SAV and the relaxed SAV are shown. The RSAV-CN scheme provides accurate result even with a much larger time step than the baseline SAV-CN scheme. In (b), the numerical results for $q(t) - Q(\phi(\mathbf{x}, t))$ are shown, where we observe that the baseline SAV introduces numerical errors for $q(t) - Q(\phi(\mathbf{x}, t))$, but the relaxed SAV method shows better consistency between q^{n+1} and $Q(\phi^{n+1})$.

$$\phi(x, y) = \tanh \frac{1.5 + 1.2\cos(6\theta) - 2\pi r}{\sqrt{2}\varepsilon}, \tag{5.4a}$$

$$\theta = \arctan \frac{y - 0.5L_y}{x - 0.5L_x}, \quad r = \sqrt{(x - \frac{L_x}{2})^2 + (y - \frac{L_y}{2})^2}. \tag{5.4b}$$

In this example, we set $L_x = L_y = 1$. We observe that the RSAV-CN method is more accurate than the baseline SAV-CN method, even with a larger time step. In addition, the numerical errors between q^{n+1} and $Q(\phi^{n+1})$ are shown in Fig. 5.2(b). We observe that the RSAV method can effectively reduce the numerical errors between q^{n+1} and $Q(\phi^{n+1})$. This is essential for preserving the consistency between the modified energy and the original energy after temporal discretization.

5.2. Cahn-Hilliard equation

In the second example, we consider the well-known Cahn-Hilliard equation with a double-well potential. Mainly, consider the free energy $\mathcal{E} = \int_\Omega \frac{\varepsilon^2}{2}|\nabla\phi|^2 + \frac{1}{4}(\phi^2 - 1)^2 d\mathbf{x}$, and mobility operator, $\mathcal{G} = -\lambda\Delta$. The general gradient flow model in (2.1) reduces to the corresponding Cahn-Hilliard equation

$$\partial_t \phi = \lambda \Delta \mu, \tag{5.5a}$$

$$\mu = -\varepsilon^2 \Delta\phi + \phi^3 - \phi. \tag{5.5b}$$

In the SAV formulation, we introduce the scalar auxiliary variable

$$q(t) := Q(\phi(\mathbf{x}, t)) = \sqrt{\int_\Omega \frac{1}{4}(\phi^2 - 1 - \gamma_0)^2 d\mathbf{x} + C}.$$

Then the reformulated equations are obtained as

$$\partial_t \phi = \lambda \Delta \mu, \tag{5.6a}$$

$$\mu = -\varepsilon^2 \Delta \phi + \gamma_0 \phi + \frac{q(t)}{Q(\phi)} V(\phi), \quad V(\phi) = \phi(\phi^2 - 1 - \gamma_0), \tag{5.6b}$$

$$\frac{d}{dt} q(t) = \int_\Omega \frac{V(\phi)}{2Q(\phi)} \partial_t \phi d\mathbf{x}. \tag{5.6c}$$

First of all, we conduct the mesh refinement tests to check the order of temporal convergence. We use the same initial condition as the AC case in (5.3) for the time mesh refinement tests. We consider the domain $\Omega = [0, 1]^2$ and model parameters $\lambda = 0.01$, $\varepsilon = 0.01$. To solve the problem, we choose the numerical parameters $C_0 = 1$, $\gamma_0 = 4$, $\eta = 0.95$, and $N_x = N_y = 128$. Then we calculate the numerical solutions to $t = 0.5$ with various time steps. The L^2 errors for numerical solutions (using strategies explained in the AC case) are calculated. The results are summarized in Fig. 5.3. A second-order temporal convergence for both ϕ and q is observed.

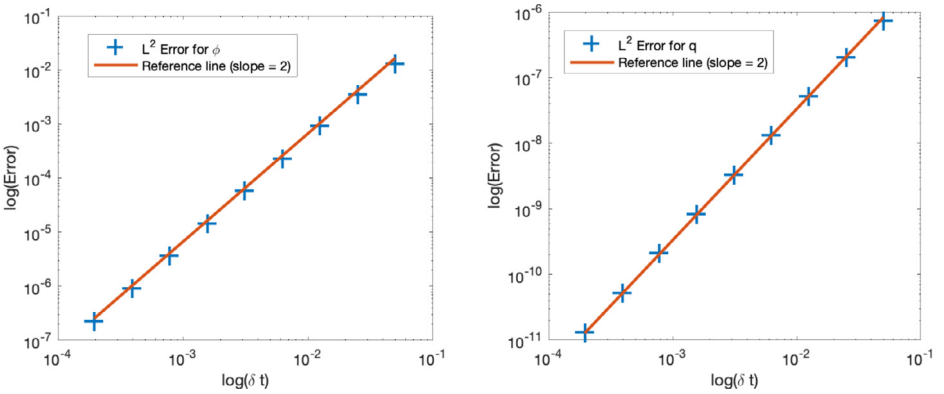

(a) Temporal mesh refinement test for ϕ (b) Temporal mesh refinement test for q

Fig. 5.3. Time step mesh refinement tests of RSAV-CN method for solving the Cahn-Hilliard equation. This figure indicates that the proposed RSAV-CN algorithm is second-order accuracy in time when solving the Cahn-Hilliard equation.

After we verify that the RSAV-CN scheme is second-order accurate, we compare the accuracy of the baseline SAV-CN scheme and the RSAV-CN scheme for solving the Cahn-Hilliard equation. We use the same initial conditions as in (5.4). The model parameters used are $\lambda = 0.1$, $\varepsilon = 0.01$, $\gamma_0 = 4$. And to solve the problem, we choose the numerical parameters $C_0 = 1$, $\eta = 0.95$, and $N_x = N_y = 128$. The comparison of calculated energies is shown in Fig. 5.4(a), and the numerical errors for $q(t) - Q(\phi(\mathbf{x}, t)))$ using both the baseline SAV-CN scheme and the relaxed SAV-CN schemes are shown in Fig. 5.4(b). We observe that the relaxation step improves the accuracy significantly. In addition, the relaxation guarantees the consistency of numerical solution q^{n+1} with its original definition $Q(\phi^{n+1})$, which indicates the numerical consistency of modified energy and the original energy.

Next, we investigate the coarsening dynamics driven by the Cahn-Hilliard equation. We consider the domain $\Omega = [0, 4]^2$, and set $\lambda = 0.1$, $\varepsilon = 0.01$. Set the initial condition as $\phi(x, y, t = 0) = \hat{\phi}_0 + 0.05 rand(x, y)$, where $rand(x, y)$ generates rand numbers between -1 and 1, and $\hat{\phi}_0$ is a constant. We use the relaxed SAV-CN scheme to solve it with meshes $N_x = N_y = 512$, model parameters $\gamma_0 = 4$, $C_0 = 1$, $\eta = 0.95$ and time step $\delta t = 0.001$. The results are summarized in Fig. 5.5. It is observed that when the volume difference between two phases is small, saying in Fig. 5.5(a), the spinodal decomposition dynamics takes place; when the volume difference between two phases is larger, saying in Fig. 5.5(b), the nucleation dynamics takes place.

5.3. Molecular beam epitaxy model with slope selection

In the next example, we consider the molecular beam epitaxy (MBE) model with slope selection. Given ϕ denoting the MBE thickness, the free energy is defined as $\mathcal{E} = \int_\Omega \frac{\varepsilon^2}{2}(\Delta\phi)^2 + \frac{1}{4}(|\nabla\phi|^2 - 1)^2 d\mathbf{x}$, with the mobility operator, $\mathcal{G} = 1$, the general gradient flow model in (2.1) is specified as the MBE model with slope selection, which reads as

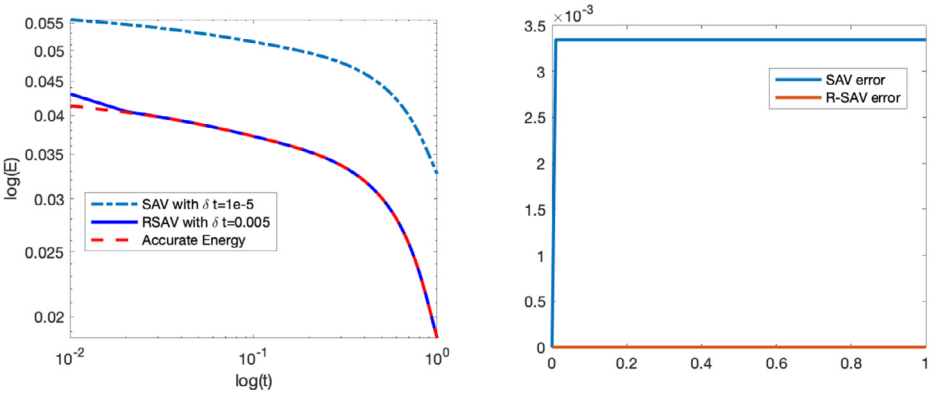

(a) Log-log plot for the energy evolution (b) Numerical results of $q(t)-Q(\phi(\mathbf{x},t))$

Fig. 5.4. A comparison between the baseline SAV method and the relaxed SAV method for solving the Cahn-Hilliard equation. In (a) the numerical energies using the baseline SAV and the relaxed SAV are shown. The RSAV method provides accurate result even with larger time step than the baseline SAV method. In (b), the numerical results for $q(t)-Q(\phi(\mathbf{x},t))$ are shown, where we observe that the baseline SAV introduces numerical errors for $q(t)-Q(\phi(\mathbf{x},t))$, but the relaxed SAV has properly relaxed the error close to 0.

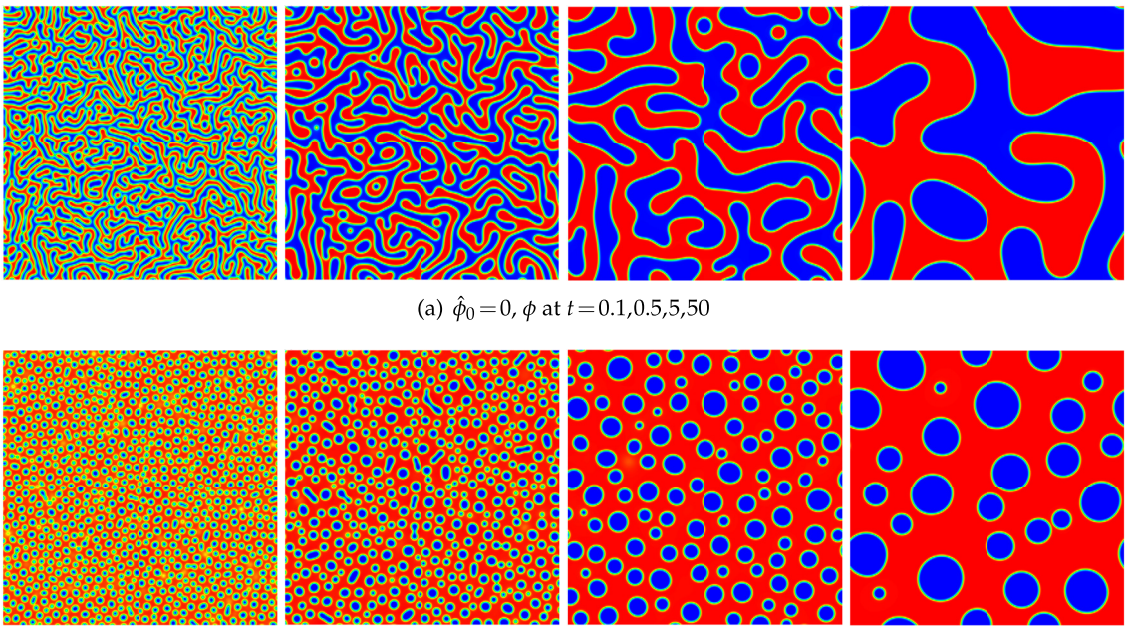

(a) $\hat{\phi}_0=0$, ϕ at $t=0.1,0.5,5,50$

(b) $\hat{\phi}_0=0.4$, ϕ at $t=0.1,0.5,5,50$

Fig. 5.5. Coarsening dynamics driven by the Cahn-Hilliard equation. In (a), we set $\hat{\phi}_0=0$, and the profiles of ϕ at $t=0.1,0.5,5,50$ are shown; (b) we set $\hat{\phi}_0=0.4$, and the profiles of ϕ at $t=0.1,0.5,5,50$ are shown.

$$\partial_t\phi=-\varepsilon^2\Delta^2\phi+\nabla\cdot(|\nabla\phi|^2-1)\nabla\phi). \tag{5.7}$$

With the similar idea as the previous examples, we introduce the scalar auxiliary variable

$$q(t):=Q(\phi(\mathbf{x},t))=\sqrt{\frac{1}{4}\int_\Omega(|\nabla\phi|^2-1-\gamma_0)^2d\mathbf{x}+C_0}, \tag{5.8}$$

then the reformulated model reads as

$$\partial_t\phi=-\varepsilon^2\Delta^2\phi+\gamma_0\Delta\phi+\nabla\cdot(\frac{q(t)}{Q(\phi)}\nabla\phi), \tag{5.9a}$$

$$\frac{d}{dt}q(t) = \int_{\Omega} \frac{\nabla\phi \cdot \nabla\partial_t\phi}{2Q(\phi)} d\mathbf{x}. \tag{5.9b}$$

As a routine, we test the temporal convergence of the relaxed SAV-CN scheme for the MBE model. Consider the domain $\Omega = [0,1]^2$, and the model parameter $\varepsilon = 0.1$. We use the same initial condition as before, i.e. $\phi(x, y, t = 0) = 0.01\cos(2\pi x)\cos(2\pi y)$. We choose $N_x = N_y = 128$, $\gamma_0 = 4$, $C_0 = 0$, and $\eta = 0.95$. The numerical errors at $t = 0.5$ are calculated and summarized in Fig. 5.6. A second-order convergence for both ϕ and q are observed, when the time step is not too large.

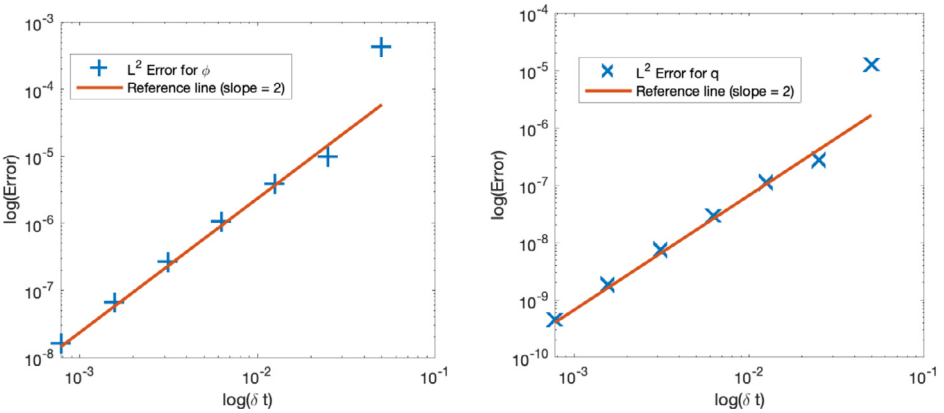

(a) time mesh refinement test for ϕ (b) time mesh refinement test for q

Fig. 5.6. Time step mesh refinement tests of RSAV-CN method for solving the MBE model. This figure indicates that the proposed RSAV-CN algorithm is second-order accuracy in time when solving the MBE model.

Then, we compare the accuracy between the baseline SAV-CN method and the relaxed SAV-CN method for solving the MBE model. We use the classical benchmark problem for the MBE model. Mainly we consider the domain $\Omega = [0, 2\pi]^2$, with $\varepsilon^2 = 0.1$. We solve the problem with $N_x = N_y = 128$, $\gamma_0 = 4$, $C_0 = 1$, $\eta = 0.95$. The numerical comparisons between the baseline SAV-CN scheme and the relaxed SAV-CN scheme are summarized in Fig. 5.7. We observe that the relaxation step increases the numerical accuracy and guarantees the numerical consistency between q^{n+1} and $Q(\phi^{n+1})$. Here we emphasize that the relaxation step is computationally negligible.

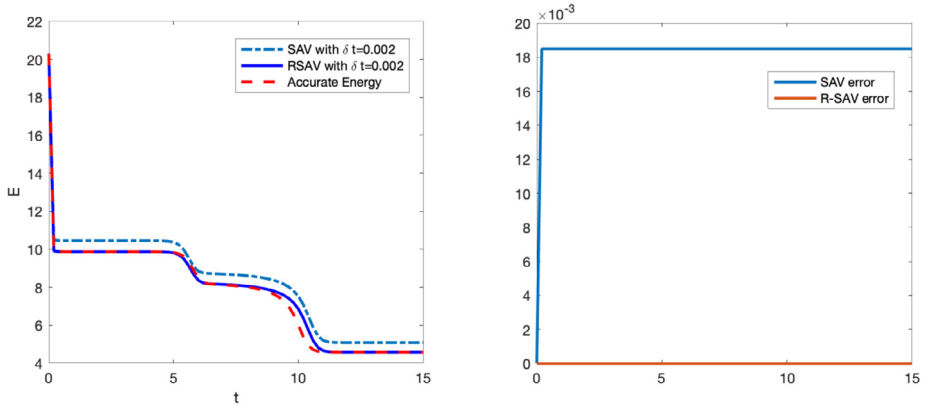

(a) Numerical energies (b) Numerical errors for $q(t) - Q(\phi(\mathbf{x}, t))$

Fig. 5.7. A comparison between the baseline SAV-CN method and the RSAV-CN method for solving the MBE model. In (a) the comparisons of numerical energies are shown. The RSAV method provides more accurate results. In (b), the numerical results for $q(t) - Q(\phi(\mathbf{x}, t))$ are shown, where we observe that the baseline SAV introduces numerical errors for $q(t) - Q(\phi(\mathbf{x}, t))$, but the relaxed SAV guarantees the consistency of $q(t)$ and $Q(\phi(\mathbf{x}, t)$ numerically.

5.4. Other phase-field models

Thanks to the SAV method's generality, the relaxed SAV method also applies to various dissipative PDE models, and particularly thermodynamically consistent phase field models. We skip some details of using the RSAV method on other models due to space limitation but focus on two more specific applications: (1) the phase-field crystal model; and (2) the diblock copolymer model.

First of all, we consider its application to the phase field crystal (PFC) model. Consider the free energy $\mathcal{E} = \int_\Omega \frac{1}{2}\phi(a_0 + \Delta)^2\phi + \frac{1}{4}\phi^4 - \frac{b_0}{2}\phi^2 d\mathbf{x}$ where a_0 and b_0 are model parameters, and the mobility operator $\mathcal{G} = -\lambda\Delta$. The general gradient flow model in (2.1) is reduced to the PFC model, which reads as

$$\partial_t \phi = \lambda \Delta \mu, \tag{5.10a}$$

$$\mu = -(a_0 + \Delta)^2\phi + \phi^3 - b_0\phi. \tag{5.10b}$$

If we introduce the scalar auxiliary variable $q(t) := Q(\phi(\mathbf{x}, t)) = \sqrt{\frac{1}{4}\int_\Omega (\phi^2 - b_0 - \gamma_0)^2 d\mathbf{x} + C_0}$, we get the reformulated model

$$\partial_t \phi = \lambda \Delta \mu, \tag{5.11a}$$

$$\mu = -(a_0 + \Delta)^2\phi + \gamma_0\phi + \frac{q(t)}{Q(\phi)}V(\phi), \quad V(\phi) = \phi(\phi^2 - b_0 - \gamma_0), \tag{5.11b}$$

$$\frac{d}{dt}q(t) = \int_\Omega \frac{V(\phi)}{2Q(\phi)}\partial_t \phi d\mathbf{x}. \tag{5.11c}$$

We verify that the RSAV scheme shows second-order convergence in time when solving the PFC model. The results are not shown to save space. Then we compare the accuracy between the baseline SAV-CN scheme and the relaxed SAV-CN scheme. We consider the domain $\Omega = [0, 400]^2$, and set $a_0 = 1$, $b_0 = 0.325$, $\lambda = 1$. To solve the PFC model, we use the numerical parameters $\gamma_0 = 1$, $C_0 = 1$, $N_x = N_y = 512$, $\eta = 0.95$. The initial condition is chosen as shown in Fig. 5.9(a). The numerical comparisons between the two schemes are summarized in Fig. 5.8. The RSAV-CN scheme shows more accurate results. Most importantly, the results obtained from the RSAV-CN method show the numerical consistency between the modified energy and the original energy, since it guarantees the consistency of $q(t)$ with $Q(\phi(\mathbf{x}, t))$ as shown in Fig. 5.8(b).

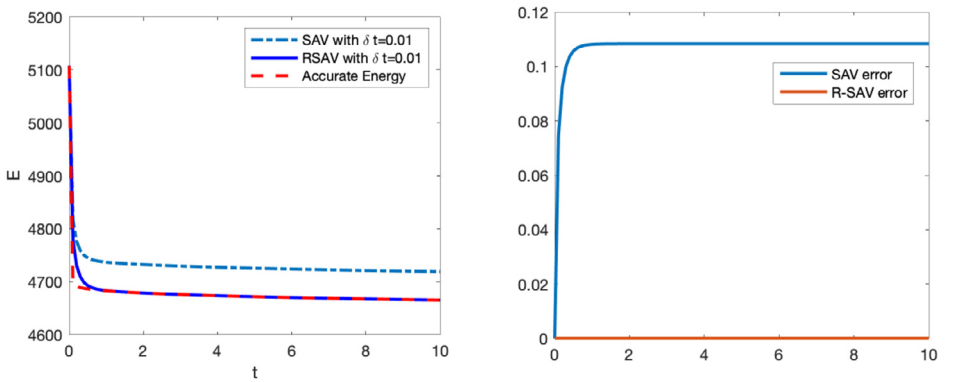

(a) Numerical energies (b) Numerical errors for $q(t) - Q(\phi(\mathbf{x}, t))$

Fig. 5.8. A comparison between the baseline SAV-CN method and the RSAV-CN method for solving the PFC model. In (a) the comparisons of numerical energies using different methods are shown. The RSAV-CN method provides more accurate results than the baseline SAV-CN method. In (b), the numerical errors for $q(t) - Q(\phi(\mathbf{x}, t))$ are shown. We observe that the baseline SAV-CN method introduces numerical errors for $q(t) - Q(\phi(\mathbf{x}, t))$, but the RSAV-CN method guarantees the consistency of $q(t)$ and $Q(\phi(\mathbf{x}, t)$ numerically.

Also, the profiles of ϕ at various times using the relaxed SAV-CN scheme with a time step $\delta t = 0.01$ are summarized in Fig. 5.9. It indicates the relaxed SAV-CN can be utilized to investigate long-time dynamics and provides accurate numerical results.

Furthermore, we use the relaxed SAV-CN scheme to investigate the dynamics driven by the PFC model. In this case, we consider the domain $\Omega = [0, 100]^2$, and choose the initial condition $\phi(x, y, t = 0) = \hat{\phi}_0 + 0.01 rand(x, y)$, where $rand(x, y)$ generates random numbers between -1 and 1 and $\hat{\phi}_0$ is a constant. To solve the PFC model, we use the numerical settings $N_x = N_y = 256$, $\gamma_0 = 1$, $C_0 = 1$. The numerical results are summarized in Fig. 5.10. The stripe pattern is observed with

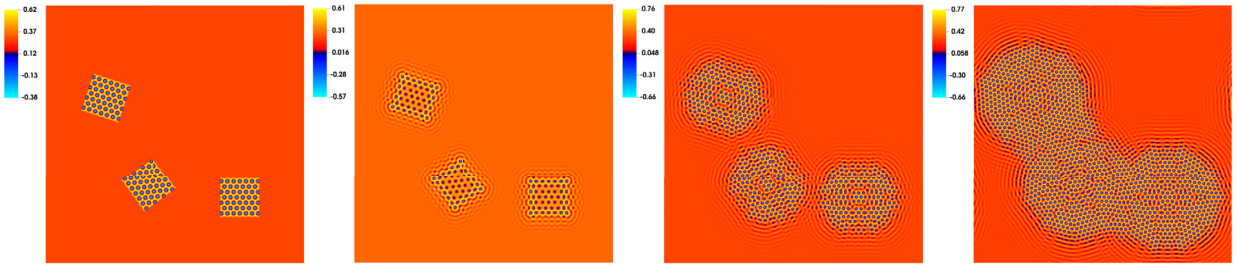

(a) ϕ at $t = 0,20,50,80$

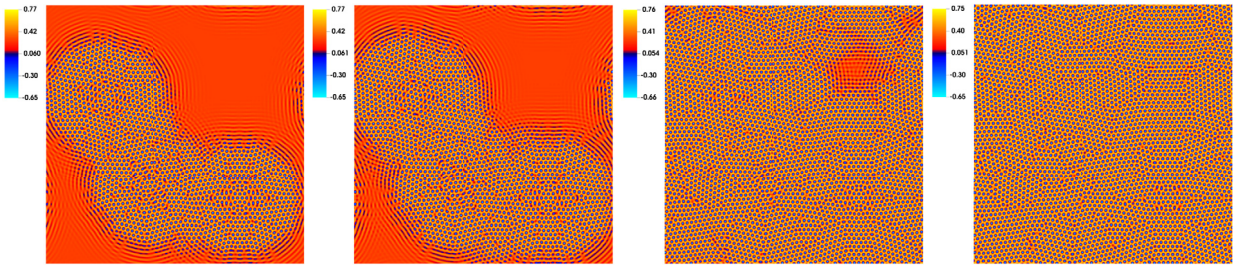

(b) ϕ at $t = 90,100,150,250$

Fig. 5.9. Crystal growth dynamics driven by the PFC model. The profiles of ϕ at various time slots are shown.

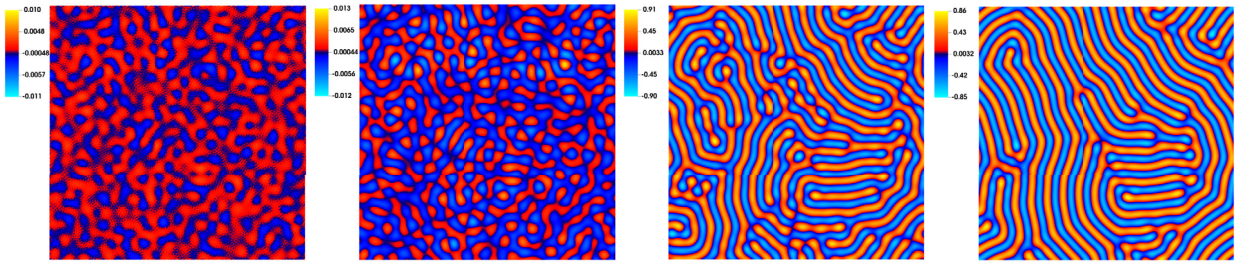

(a) ϕ at $t = 1,5,50,200$ with $\hat{\phi}_0 = 0$

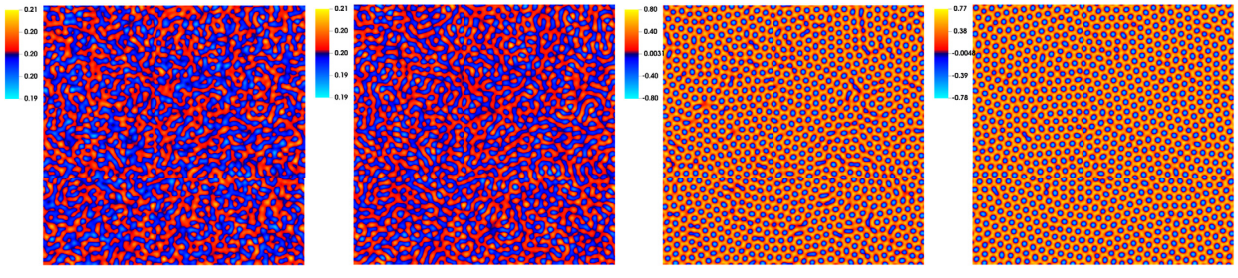

(b) ϕ at $t = 1,5,50,200$ with $\hat{\phi}_0 = 0.2$

Fig. 5.10. Crystal growth pattern formation with different initial conditions governed by the PFC model. (a) $\hat{\phi}_0 = 0$; (b) $\hat{\phi}_0 = 0.2$.

$\hat{\phi}_0 = 0$, and the triangle pattern is observed with $\hat{\phi}_0 = 0.2$. These observations are consistent with phase diagram of the PFC model as reported in the literature.

In the last example, we examine the diblock copolymer model with the proposed RSAV method. Consider the free energy

$$\mathcal{E} = \int_\Omega \frac{\varepsilon^2}{2}|\nabla\phi|^2 + \frac{1}{4}(\phi^2-1)^2 d\mathbf{x} + \frac{\sigma}{2}\int_\Omega\int_\Omega G(\mathbf{x}-\mathbf{y})(\phi(\mathbf{x})-\hat{\phi}_0)(\phi(\mathbf{y})-\hat{\phi}_0)d\mathbf{x}d\mathbf{y}$$

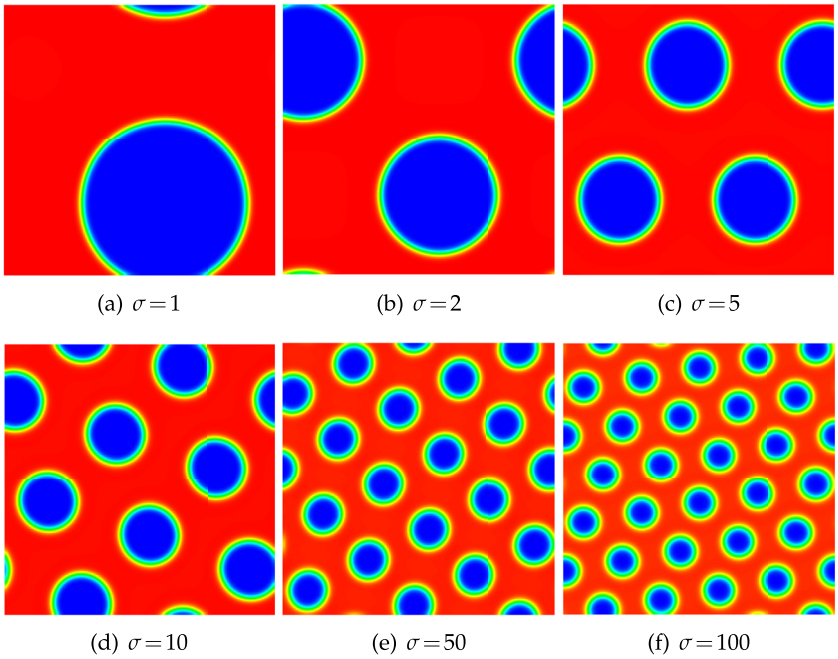

Fig. 5.11. Coarsening dynamics driven by the diblock copolymer model. The profiles of ϕ at $t=500$ are shown under various nonlocal interactions strength σ. It shows that more droplets are formed with stronger nonlocal interaction strength σ.

with σ a parameter for the nonlocal interaction strength and the mobility operator $\mathcal{G}=-\lambda\Delta$. Here G is the Green's function such that $\Delta G(\mathbf{x}-\mathbf{y})=-\delta(\mathbf{x}-\mathbf{y})$ with periodic boundary conditions and δ is a Dirac delta function. The general gradient flow model in (2.1) is specified into the phase-field diblock-copolymer model, which reads as

$$\partial_t\phi=\lambda\Big[\Delta\mu-\sigma(\phi-\hat{\phi}_0)\Big], \tag{5.12a}$$

$$\mu=-\varepsilon^2\Delta\phi+\phi^3-\phi. \tag{5.12b}$$

We consider a domain $\Omega=[0,1]^2$, and parameters $\lambda=0.1$, $\varepsilon=0.01$, $\hat{\phi}_0=0.4$, and initial condition $\phi(x,y,t=0)=\hat{\phi}_0+0.05rand(x,y)$ where $rand(x,y)$ generates random numbers in the range $[-1,1]$. To solve the model, we use the numerical parameters $\gamma_0=4$, $C_0=1$, $N_x=N_y=128$. Here we test various nonlocal interaction strength σ. The numerical results at $t=500$ are summarized in Fig. 5.11. We observe that the number of droplets scales with the nonlocal interaction strength σ.

6. Conclusion

In this paper, we introduce a relaxation technique to improve the accuracy and consistency of the baseline SAV method for solving dissipative PDE models (phase-field models in particular). Our relaxed-SAV (RSAV) approach leads to linear, second-order, unconditionally energy stable numerical schemes. Most importantly, the RSAV schemes preserve the original energy given the relaxation parameter ξ reaches 0. Furthermore, we provide detailed proofs for the energy stability properties of the RSAV method. Then, we apply the RSAV method to solve the Allen-Cahn (AC) equation, the Cahn-Hilliard (CH) equation, the Molecular Beam Epitaxy (MBE) model, the phase-field crystal (PFC) model, and the diblock copolymer model. Numerical experiments highlight the accuracy and efficiency of the proposed RSAV method. The numerical comparisons between the baseline SAV schemes and the RSAV schemes indicate that the RSAV method is unconditionally energy stable according to the original energy law and has better accuracy and consistency over the baseline SAV method.

Declaration of competing interest

The authors declare that they have no known competing financial interests or personal relationships that could have appeared to influence the work reported in this paper.

Acknowledgements

Z. Zhang and J. Zhao would like to acknowledge the support from the National Science Foundation (NSF) USA with DMS-1816783 and DMS-2111479. M. Jiang's work was supported partially by the Natural Science Foundation of Shandong Province(Grant number ZR2021QA018).

References

[1] G. Akrivis, B. Li, D. Li, Energy-decaying extrapolated RK–SAV methods for the Allen–Cahn and Cahn–Hilliard equations, SIAM J. Sci. Comput. 41 (6) (2019) A3703–A3727.
[2] D.M. Anderson, G.B. McFadden, A.A. Wheeler, A diffuse diffusion method in fluid mechanics, Annu. Rev. Fluid Mech. 30 (1998) 139–165.
[3] X. Antoine, J. Shen, Q. Tang, Scalar auxiliary variable/Lagrange multiplier based pseudospectral schemes for the dynamics of nonlinear Schrödinger/Gross-Pitaevskii equations, J. Comput. Phys. 437 (2021) 110328.
[4] S. Badia, F. Guillén-González, J.V. Gutiérrez-Santacreu, Finite element approximation of nematic liquid crystal flows using a saddle-point structure, J. Comput. Phys. 230 (2011) 1686–1706.
[5] A. Barrett, J.S. Lowengrub, C. Wang, S.M. Wise, Convergence analysis of a second order convex splitting scheme for the modified phase field crystal equation, SIAM J. Numer. Anal. 51 (2013) 2851–2873.
[6] L. Chen, J. Zhao, Y. Gong, A novel second-order scheme for the molecular beam epitaxy model with slope selection, Commun. Comput. Phys. 25 (2019) 1024–1044.
[7] L. Chen, J. Zhao, X. Yang, Regularized linear schemes for the molecular beam epitaxy model with slope selection, Appl. Numer. Math. 128 (2018) 1876–1892.
[8] K. Cheng, Z. Qiao, C. Wang, A third order exponential time differencing numerical scheme for no-slope-selection epitaxial thin film model with energy stability, Commun. Comput. Phys. 81 (2019) 154–185.
[9] Q. Cheng, J. Shen, Multiple scalar auxiliary variable (MSAV) approach and its application to the phase field vesicle membrane model, SIAM J. Sci. Comput. 40 (2018) A3982–A4006.
[10] H. Zhu, D. Hou, C. Xu, Highly efficient schemes for time-fractional Allen-Cahn equation using extended sav approach, Numer. Algorithms 88 (2021) 1077–1108.
[11] M. Doi, S.F. Edwards, The Theory of Polymer Dynamics, vol. 73, Oxford University Press, 1988.
[12] K. Elder, M. Grant, Modeling elastic and plastic deformations in nonequilibrium processing using phase field crystals, Phys. Rev. E 70 (051605) (2004).
[13] D.J. Eyre, Unconditionally gradient stable time marching the Cahn-Hilliard equation, Mrs Online Proceedings Library Archive 529 (1998) 39–46.
[14] X. Feng, B. Li, S. Ma, High-order mass- and energy-conserving SAV-Gauss collocation finite element methods for the nonlinear Schrödinger equation, SIAM J. Numer. Anal. 59 (3) (2021) 1566–1591.
[15] X. Feng, A. Prohl, Error analysis of a mixed finite element method for the Cahn-Hilliard equation, Numer. Math. 99 (2004) 47–84.
[16] M.G. Forest, Q. Wang, R. Zhou, The flow-phase diagram of Doi-Hess theory for sheared nematic polymers II: finite shear rates, Rheol. Acta 44 (2004) 80–93.
[17] M.G. Forest, Q. Wang, R. Zhou, The weak shear kinetic phase diagram for nematic polymers, Rheol. Acta 43 (2004) 17–37.
[18] J.G.E.M. Fraaije, Dynamic density functional theory for microphase separation kinetics of block copolymer melts, J. Chem. Phys. 99 (9202) (1993).
[19] L. Giacomelli, F. Otto, Variational formulation for the lubrication approximation of the Hele-Shaw flow, Calc. Var. Partial Differ. Equ. 13 (2001) 377–403.
[20] Y. Gong, J. Zhao, Energy-stable Runge-Kutta schemes for gradient flow models using the energy quadratization approach, Appl. Math. Lett. 94 (2019) 224–231.
[21] Y. Gong, J. Zhao, Q. Wang, Arbitrarily high-order unconditionally energy stable schemes for thermodynamically consistent gradient flow models, SIAM J. Sci. Comput. 42 (2020) 135–156.
[22] Y. Gong, J. Zhao, Q. Wang, Structure-preserving algorithms for the two- dimensional Sine-Gordon equation with Neumann boundary conditions, Comput. Phys. Commun. 249 (2020) 107033.
[23] F. Guillén-González, G. Tierra, On linear schemes for a Cahn-Hilliard diffuse interface model, J. Comput. Phys. 234 (2013) 140–171.
[24] Z. Guo, F. Yu, P. Lin, S.M. Wise, J. Lowengrub, A diffuse domain method for two-phase flows with large density ratio in complex geometries, J. Fluid Mech. 907 (A38) (2021).
[25] D. Hou, M. Azaiez, C. Xu, A variant of scalar auxiliary variable approaches for gradient flows, J. Comput. Phys. 395 (2019) 307–332.
[26] F. Huang, J. Shen, Z. Yang, A highly efficient and accurate new SAV approach for gradient flows, SIAM J. Sci. Comput. 42 (2020) A2514–A2536.
[27] J. Kim, J. Yang, A variant of stabilized-scalar auxiliary variable (S-SAV) approach for a modified phase-field surfactant model, Comput. Phys. Commun. 261 (2021) 107825.
[28] B. Ji, H. Liao, Y. Gong, L. Zhang, Adaptive second-order Crank–Nicolson time-stepping schemes for time-fractional molecular beam epitaxial growth models, SIAM J. Sci. Comput. 32 (3) (2020) B738–B760.
[29] L. Ju, X. Li, Z. Qiao, H. Zhang, Energy stability and error estimates of exponential time differencing schemes for the epitaxial growth model without slope selection, Math. Comput. 87 (2018) 1859–1885.
[30] X. Li, J. Shen, On a SAV-MAC scheme for the Cahn-Hilliard-Navier-Stokes phase field model and its error analysis for the corresponding Cahn-Hilliard-Stokes case, Math. Models Methods Appl. Sci. 30 (2020) 2263–2297.
[31] X. Li, J. Shen, H. Rui, Energy stability and convergence of SAV block-centered finite difference method for gradient flows, Math. Comput. 88 (2019) 2047–2068.
[32] X. Li, J. Shen, H. Rui, Error analysis of the SAV-MAC scheme for the Navier-Stokes equations, SIAM J. Numer. Anal. 58 (2020) 2465–2491.
[33] C. Liu, J. Shen, X. Yang, Dynamics of defect motion in nematic liquid crystal flow: modeling and numerical simulation, Commun. Comput. Phys. 2 (2007) 1184–1198.
[34] Z. Qiao, S. Sun, T. Zhang, Y. Zhang, A new multi-component diffuse interface model with Peng-Robinson equation of state and its scalar auxiliary variable (SAV) approach, Commun. Comput. Phys. 26 (2019) 1597–1616.
[35] J. Shen, C. Wang, X. Wang, S.M. Wise, Second-order convex splitting schemes for gradient flows with Ehrlich-Schwoebel type energy: application to thin film epitaxy, SIAM J. Numer. Anal. 50 (2012) 105–125.
[36] J. Shen, J. Xu, J. Yang, The scalar auxiliary variable (SAV) approach for gradient flows, J. Comput. Phys. 353 (2018) 407–416.
[37] J. Shen, J. Xu, J. Yang, A new class of efficient and robust energy stable schemes for gradient flows, SIAM Rev. 61 (2019) 474–506.
[38] C. Wang, X. Wang, S.M. Wise, Unconditionally stable schemes for equations of thin film epitaxy, Discrete Contin. Dyn. Syst. 28 (1) (2010) 405–423.
[39] C. Wang, S.M. Wise, An energy stable and convergent finite-difference scheme for the modified phase field crystal equation, SIAM J. Numer. Anal. 49 (2011) 945–969.
[40] X. Wang, L. Ju, Q. Du, Efficient and stable exponential time differencing Runge-Kutta methods for phase field elastic bending energy models, J. Comput. Phys. 316 (2016) 21–38.

[41] C. Xu, T. Tang, Stability analysis of large time-stepping methods for epitaxial growth models, SIAM J. Numer. Anal. 2 (2006) 1759–1779.
[42] X. Yang, J. Zhao, X. He, Linear, second order and unconditionally energy stable schemes for the viscous Cahn-Hilliard equation with hyperbolic relaxation, J. Comput. Appl. Math. 343 (2018) 80–97.
[43] X. Yang, J. Zhao, Q. Wang, Numerical approximations for the molecular beam epitaxial growth model based on the invariant energy quadratization method, J. Comput. Phys. 333 (2017) 102–127.
[44] X. Yang, J. Zhao, Q. Wang, J. Shen, Numerical approximations for a three components Cahn-Hilliard phase-field model based on the invariant energy quadratization method, Math. Models Methods Appl. Sci. 27 (2017) 1993–2023.
[45] P. Yue, J. Feng, C. Liu, J. Shen, A diffuse-interface method for simulating two phase flows of complex fluids, J. Fluid Mech. 515 (2004) 293–317.
[46] J. Zhao, Q. Wang, X. Yang, Numerical approximations for a phase field dendritic crystal growth model based on the invariant energy quadratization approach, Int. J. Numer. Methods Eng. 110 (2017) 279–300.
[47] J. Zhao, X. Yang, Y. Gong, Q. Wang, A novel linear second order unconditionally energy stable scheme for a hydrodynamic-tensor model of liquid crystals, Comput. Methods Appl. Mech. Eng. 318 (2017) 803–825.
[48] J. Zhao, X. Yang, Y. Gong, X. Zhao, X. Yang, J. Li, Q. Wang, A general strategy for numerical approximations of non-equilibrium models part I thermodynamical systems, Int. J. Numer. Anal. Model. 15 (6) (2018) 884–918.
[49] J. Zhao, A revisit of the energy quadratization method with a relaxation technique, Appl. Math. Lett. 120 (2021) 107331.
[50] G. Zhu, J. Kou, S. Sun, J. Yao, A. Li, Numerical approximation of a phase-field surfactant model with fluid flow, J. Sci. Comput. 80 (2019) 223–247.